Defence Science Journal, Vol. 65, No. 1, January 2015, pp. 12-24, DOI : 10.14429/dsj.65.7200

Optimised Cockpit Heat Load Analysis using Skin Temperature Predicted by CFD and Validation by Thermal Mapping to Improve the Performance of Fighter Aircraft

Paresh Gupta[*] and S.P.S. Rajput[#]

[*]*Aircraft Upgrade Research and Design Centre, Hindustan Aeronautics Ltd, Nasik - 422 207, India*
[#] *Maulana Azad National Institute of Technology, Bhopal - 462 051, India*
[*]*E-mail: pareshgupta1977@gmail.com*

ABSTRACT

Designing of optimum environmental control system (ECS) plays a major role for increasing performance of fighter aircraft depending upon requirement of engine bleed air for running of ECS. Accurate estimation of cockpit skin temperature for obtaining optimised cockpit heat load helps in estimation of engine bleed air for ECS. Present research evolved a methodology for comparing the theoretically calculated skin temperature with computational fluid dynamics (CFD) analysis to obtain optimum skin temperature. Results are validated by flight tests under critical flight conditions using thermal crayons. Based on which the optimized heat load and bleed air requirements has been computed. Uncertainty analysis of skin temperature measurement for thermal crayons have been undertaken. The results indicate that the theoretical skin temperature is -26.70 per cent as that of CFD estimated skin temperature. Optimized average cockpit heat load at critical flight profiles is 0.74 times the theoretical cockpit heat load, leading to reduction of bleed air requirement by 26 per cent as compared to theoretical. Due to this literature survey has pridicted the increase in performance parameters like increase in bleed air pressure by 78 per cent, increase in thrust by 60 per cent, and decrease in specific fuel consumption (SFC) by 40 per cent to improve the endurance of aircraft. The research has generated governing equations for variation of cockpit heat loads w.r.t aircraft skin temperatures.

Keywords: Environmental control system, computational fluid dynamics, cockpit heat load analyses

NOMENCLATURE

A_{bulk}	Front bulkhead area
A_{rbulk}	Rear bulkhead area
A_{flr}	Floor area
A_{proj}	Area of projections
A_{ws}	Windshield surface area
A_{cpy}	Canopy surface area
b_{bulk}	Thickness of front bulkhead
b_{flr}	Thickness of floor
$b_{perspex}$	Thickness of windshield
b_{canopy}	Thickness of canopy
b_{bulk}	Thickness of front bulkhead
C_p	Specific heat of air at constant pressure (kJ/kg K)
C_f	Coefficient of friction
Gv	Production of turbulent viscosity
h_{gr}	Heat transfer coefficient due to radiation
h_{gc}	Heat transfer coefficient due to convection
k_{bulk}	Thermal conductivity of front bulkhead
h_o	Stagnation enthalpy
h_∞	Enthalpy of free stream air.
K	Thermal conductivity of free stream air
k_{bulk}	Thermal conductivity of front bulkhead
k_{flr}	Thermal conductivity of floor
$k_{perspex}$	Thermal conductivity of canopy
k_{ws}	Thermal conductivity of windshield
m	Mass flow rate of cooling air supplied (kg/s)
M	Mach No
T_{skin}	Skin temperature
T_∞	Ambient temperature
T_{cabin}	Temperature to be maintained inside the cockpit
$T_{supplied}$	Temperature of supplied cooling air
T_{aw}	Adiabatic wall temperature
T^*	Reference temperature
S_t	Stanton number
P_r	Prandtl number
$LRUs$	Line replaceable units
Q_{th}	Theoretical cockpit heat load
SFC	Specific fuel consumption
CFD	Computational fluid dynamics
ACS	Air conditioning system
AoA	Angle of attack

Overall coefficient of heat transfer

U_1	through cockpit side wall
U_2	through front bulkhead
U_3	through rear bulkhead
U_4	through cockpit floor
U_5	through structural projections
U_6	through windshield
U_7	through canopy

Received 14 May 2014, revised 7 December 2014, online published 27 February 2015

Estimated cockpit heat loads by
$(Q_{FP1})_{CFD}$ CFD analysis for flight profile 1
$(Q_{FP2})_{CFD}$ CFD analysis for flight profile 2
$(Q_{FP3})_{CFD}$ CFD analysis for flight profile 3

Estimated cockpit heat loads by
$(Q_{FP1})_{FT1}$ flight test 1 for flight profile 1
$(Q_{FP2})_{FT2}$ flight test 2 for flight profile 2
$(Q_{FP3})_{FT3}$ flight test 3 for flight profile 3
m_{th} Theoretical bleed air requirement

Bleed air requirement using cockpit heat load
$(m_{FP1})_{CFD}$ estimated by CFD for flight profile 1
$(m_{FP2})_{CFD}$ estimated by CFD for flight profile 2
$(m_{FP3})_{CFD}$ estimated by CFD for flight profile 3

Bleed air requirement using cockpit heat load
$(m_{FP1})_{FT1}$ estimated by flight test 1
$(m_{FP1})_{FT2}$ estimated by flight test 2
$(m_{FP1})_{FT3}$ estimated by flight test 3

1. INTRODUCTION

Aircraft designers are concerned to maintain the temperature of cockpit in all flight profiles as per human comfort level within specified tolerance. Major heat load generated inside the cockpit is due to the skin friction of air at high speeds. Hence, it becomes important to calculate skin temperature accurately. A precise calculation of cockpit heat load requires estimation of aircraft structure geometrical area and various parameters involved in the mechanism of heat transfer. Depending upon maximum cockpit heat load, to maintain the desired cockpit temperature, the mass flow rate of cooling air and its temperature, when it enters into cockpit, is estimated. If we overestimate the cockpit heat loads, then to maintain desired cockpit temperature, there is a requirement of high mass flow rate and low temperature inlet to cockpit. This leads to over-designing of ACS LRUs. This makes ACS LRUs bulky. Hence weight penalty is imposed on aircraft. To counter this weight penalty, requirement of high thrust engine arises, which imposes further fuel penalty on aircraft. Present practice of aircraft environmental control system (ECS) designers is to take theoretical skin temperature as a reference temperature at critical flight profiles to estimate the cockpit heat loads as a conservative approach leading to over-designing of ECS LRUs which makes ACS LRUs bulky. As a result, there is deterioration in the performance of aircraft. Authors have wide experience in designing of ECS of fighter aircraft.

The fact of over-designing of ECS LRUs by industry was a point of worry to authors. This fact has motivated the authors to carry out research for calculating optimum cockpit heat load using optimised skin temperature estimation by CFD and flight trials so that bleed air requirement can be reduced to improve the performance of aircraft. As the research is new to the aerospace industry it will give a way to ECS designers in future to reduce the bleed air penalty to improve the performance of aircraft. As skin temperature is a vital parameter for heat load calculations, optimised skin temperature has been calculated using CFD in three critical flight profiles in our previous research by Gupta and Rajput[1]. The current research has been divided into six major segments; verification of theoretical and CFD results of skin temperature by conducting flight tests at critical flight profiles using thermal crayons; calculation of optimised heat load using skin temperature derived from CFD analyses and flight tests as input parameter, generation of governing equation of variation of cockpit heat load w.r.t skin temperature for critical flight profiles; estimation of bleed air based on optimised heat load; generation of relationships between maximum possible bleed air requirement by theoretical analysis, estimated bleed air requirements by CFD analyses, and flight tests analyses for critical flight profiles; and finally prediction for the improvement in performance parameters like increase in bleed air pressure, increase in thrust, and decrease in specific fuel consumption.

2. VALIDATION OF THEORETICAL AND CFD RESULTS OF SKIN TEMPERATURE

By Flight tests at critical flight profiles using Thermal Crayons (Tempilstik indicators).

2.1 Theoretical Estimation of Skin Temperature

As per our previous research by Gupta[1], *et al*., at 313 K ambient temperature and 0.8 Mach No, the theoretical skin temperatures have been calculated as:

T_{skin} = 353.064 K (adiabatic heating due to stagnation of fluid)
= 337.708 K (heating effect due to viscous dissipation using constant property heat transfer equation at reference temperature T* as reported by Eckert[2]).

2.2 CFD Analysis to Estimate of Skin Temperature

The average skin temperature of cockpit surface has been calculated based on CFD analysis at following critical flight profiles as per our previous research[1].

Flight Profile 1: 313 K (40 °C) ambient temperature, 0.8 Mach No and 0° Angle of Attack
Flight Profile 2: 313 K (40 °C) ambient temperature, 0.8 Mach No and -7° Angle of Attack
Flight Profile 3: 313 K (40 °C) ambient temperature, 0.8 Mach No at +7° Angle of Attack

The main stages involved in CFD analysis were generation of 3-D geometry of cockpit in CATIA V5; tetrahedral meshing in hemi-spherical computational domain, processing of meshed geometry in fluent R14; post-processing of fluent data to analyse the results. Computational domain was meshed considering boundary layer formation. 3-D geometries of cockpit side walls, cone and canopy have been modeled and integrated to make complete 3-D geometry of cockpit, as shown in Fig. 1.

Spherical computational domain of size 80 m, which is approximately 41 times the radius of cockpit (1.93 m) or ≅10 times the length of cockpit (8.5 m) zone has been created for meshing For aero wall Y+=10 (a non-dimensional distance from wall to first grid point) is selected based on study of literature by Cheong[3] for low Reynolds numbers and high Reynolds numbers suitable for our application as our focus was concentrated in the buffer layer [$5 < y+ < 30$]. As flow over the skin of cockpit is turbulent ($Re > 10^6$), turbulent models with the flow in the boundary layer were considered. Boundary

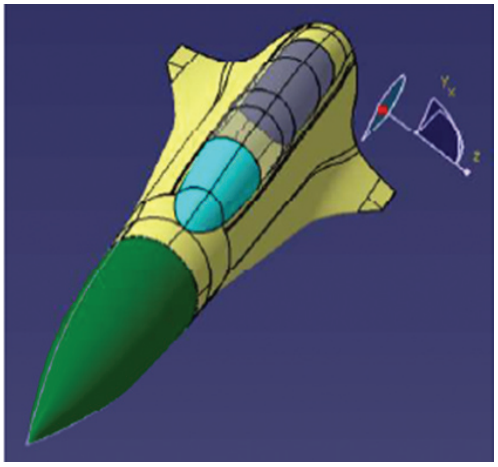

Figure 1. 3-D model of cockpit geometry with nose cone.

conditions i.e boundary wall was assigned for cockpit and pressure far-field for the domain's outer edge. Symmetry was assigned for the central plane of hemispherical computational domain. Tetrahedral meshing was created from cockpit is outer skin (geometry) to the end of computational domain. Spherical computational domain and tetrahedral meshing above cockpit surface in hemispherical computational domain are shown in Fig. 2.

The analysis was carried out on computational power from a HP Z800 workstation having Intel (R) Xeon ® CPU X5690 @ 3.47 GHz (2 processors of 6 core each) with a CPU time of about 12-14 hr for full convergence, (convergence is deemed to occur when the scaled residual in the equations fall below 10^{-8}). Grid independence study was done for optimising the solution accuracy and solution runtime. Several trial runs were carry out to find the first cell distance close to the wall. Once the grid was finalized, all meshes were run with the same boundary conditions to determine variations in flow structure and other parameters. After meshing fluent R14 workbench, necessary boundary conditions were applied for further simulation in fluent solver. The properties of fluid were defined as ideal gas. The viscosity of the air is defined as per Sutherland turbulent model with three-coefficient method. Sutherland law for viscosity is well-suited for high-speed compressible flows. Using Sutherland model, density and viscosity were made temperature-dependent but C_p and thermal conductivity were assumed constant. The strain/vorticity-based Spalart-Allmaras viscous model was selected as it was designed specifically for aerospace applications.

In this model, near wall gradients of transported variables are much smaller than the gradients of transported variables in K-ε and K-ω models. This makes the model less sensitive to numerical errors when non-layered meshes are used near wall which is a preferred choice for aerospace application. Fluent code analysed that Spalart-Allmaras model involving wall-bounded flows has been shown to give good results for boundary layers subjected to adverse pressure gradients. Pressure-based solver for the model has been selected as it yields good results for high-speed aerodynamics with shocks. Green-Gauss node-based solution was selected. This option uses better numeric on unstructured meshes. Implicit method was selected to get convergence. Unsteady method was selected for dynamic (varying with time) simulation. The following transport equation for transported variable υ' in the Spalart-Allmaras model is used:

$$\partial/\partial t\,(\rho\upsilon') + \partial/\partial xi\,(\rho\upsilon' ui) = G\upsilon + 1/\sigma\upsilon\,[\partial/\partial xj\,\{(\mu + \rho\upsilon')\,\partial\upsilon'/\partial xj\} + Cb_2\rho(\partial\upsilon'/\partial xj)2] - Y\upsilon + S\upsilon'$$

where υ' is identical to turbulent kinematic viscosity except in the near-wall (viscous affected) region. *Gv* is the production of turbulent viscosity and *Yv* is the destruction of turbulent viscosity that occurs in the near wall region due to wall blocking and viscous damping. σv and Cb_2 are constants and *v* is the molecular kinematic viscosity. *Sv* is a user defined source term.

Model constants: Cb_1=0.1355, Cb_2=0.622, Cv_1 =7.1, Cw_2=0.3 (Fluent default values).

These default values have been determined by fluent from experiments with air and water for well-bounded flows. These have been found to work fairly well with wide range of well bounded and free shear. To estimate the skin temperatures at particular point using CFD, the skin temperature at a specified 8584 nodes placed at a particular (X,Y,Z) coordinate covering entire cockpit surface have been extracted. At a particular flight condition, average of stagnation temperature has been taken to estimate the cockpit mean temperature .Using this methodology,

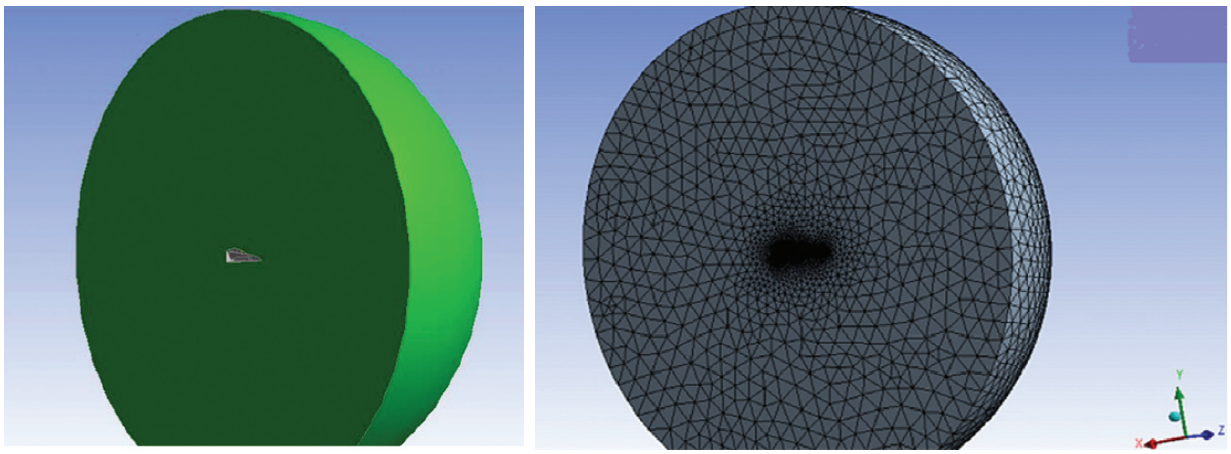

Figure 2. Spherical computational domain and tetrahedral meshing above cockpit surface in hemispherical computational domain.

average skin temperature at flight profiles 1, 2, and 3 were estimated as 320.6 K, 320.82 K, and 320.5 K, respectively. The temperature contours at flight profiles 1, 2, and 3 are shown in Fig. 3. Study of skin temperature shows that temperature is maximum at the centreline of aircraft at nose tip (343 K) and at the entrance of wind shield as these areas are subjected to adiabatic heating. Further, there is a downward trend from nose tip to aft of nose tip. The skin temperature further increases at the entrance of windshield but there is a decrease in temperature at the canopy section. Average temperature at the cockpit skin is more than at canopy skin while average temperature at fin portion is more than cockpit skin.

The comparison of result with variable angle of attack (AoA) at a particular Mach number shows that there is increase in average skin temperature as AoA changes from +7° to 0°. Further, there is an increase in average skin temperature as AoA changes from 0° AoA to -7° AoA. Comparison of skin at flight profiles 1, 2, and 3 show that maximum temperature at a particular Mach no. is at near to centre line of aircraft at -7° AoA at nose section. These results clearly show that skin temperature is highest at -7° AoA and lowest at +7° AoA. Skin temperature at 0°AoA lies in between +7° and -7° AoA. Through analyses we have identified the zone of maximum heating at a particular Mach number and AoA of aircraft. There is slight variation in skin temperature at angle of attack -7 degree and +7°. Effect is angle of attack is not significant due to approximately similar viscous heating due to shear boundary layer formation at -7° and +7° angle of attack.

2.3 Flight Tests for Thermal Mapping of Cockpit Skin

The flight tests were conducted at ambient temperature of approx. 313 K (40 °C) , speed 0.8 Mach No and angle of attack 0, -7 and +7° AoA as per flight profiles 1, 2, and 3 to measure the outer skin temperature of cockpit at specified locations. Heat-sensitive thermal crayons 'Tempilstik Indicators' manufactured by Tempil, USA were used to measure the skin temperature. 'Tempilstik indicators' make a distinct mark by melting at the point of contact once the surface reaches the product's rated temperature. These indicators are reliably accurate which melts with in ±1 per cent of the rated temperature. Temperature mapping at critical locations like: aft of nose tip, nose cone, entrance of windshield, cockpit skin, windshield, canopy, aft of cockpit, and fin portion, has been carried out using thermal crayons to compare the results w.r.t CFD analyses. Thermal crayons of temperatures 38 °C, 40 °C, 43 °C, 48 °C, 50 °C, 52 °C, 55 °C, 60 °C, 66 °C, 70 °C, 73 °C, 75 °C, 76 °C, 79 °C, and 80 °C have been selected. Lines drawn by thermal crayons are identified by writing the respective temperature near to that line in the order of increasing temperature. Expected temperature derived from theoretical and CFD analyses have been taken as benchmark to select correct range of temperature of thermal crayons. The thermal crayons ('Tempilstik indicators') and sample marking line of 50 °C, 52 °C, 55 °C and 60 °C at the entrance of windshield are shown in Fig. 4. The sample marking lines of 50 °C, 60 °C, 66 °C, and 70 °C at location aft of nose tip are shown in Fig. 5.

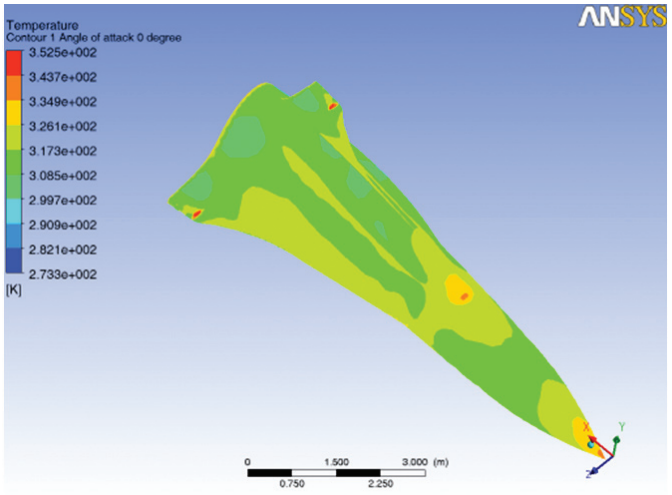

(a)

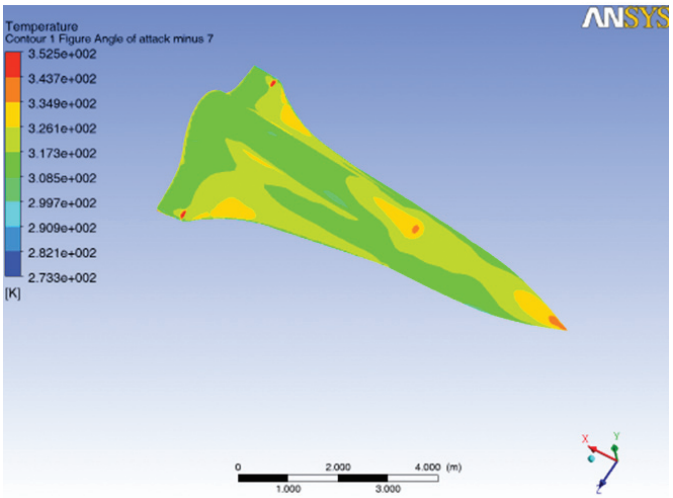

(b)

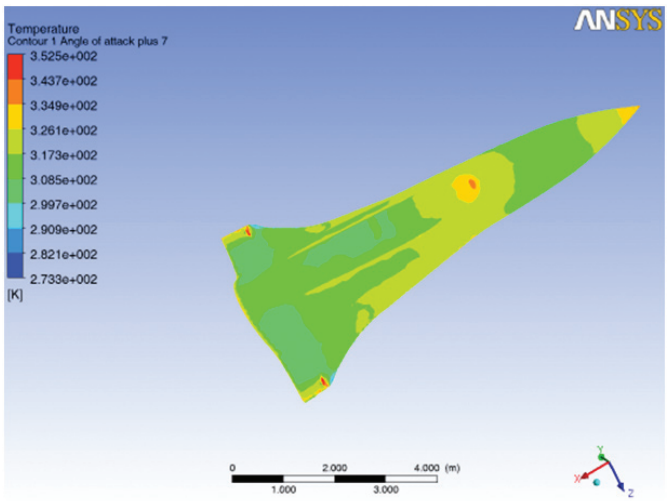

(c)

Figure 3. Temperature contour at flight profiles 1, 2 and 3: (a) Temperature contour at 313 K, 0.8 Mach No and 0° angle of attack, (b) Temperature contour at 313 K, 0.8 Mach No and -7° angle of attack, and (c) Temperature contour at 313 K, 0.8 Mach No and +7° angle of attack.

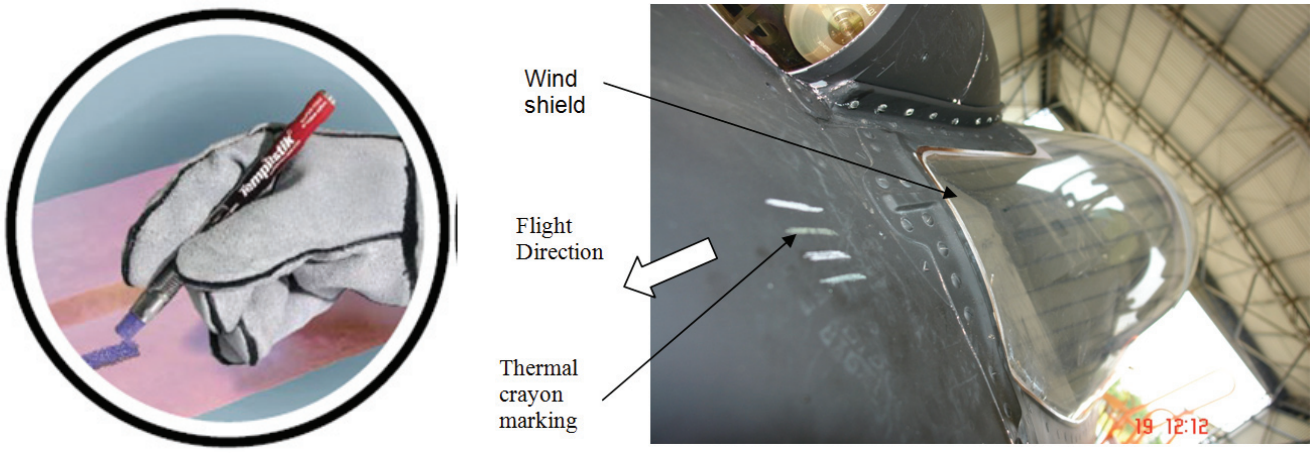

Figure 4 . (a) Thermal crayon (Tempil Stick Indicators) and (b) sample thermal crayon marking on skin near to wind shield (flight profile 1).

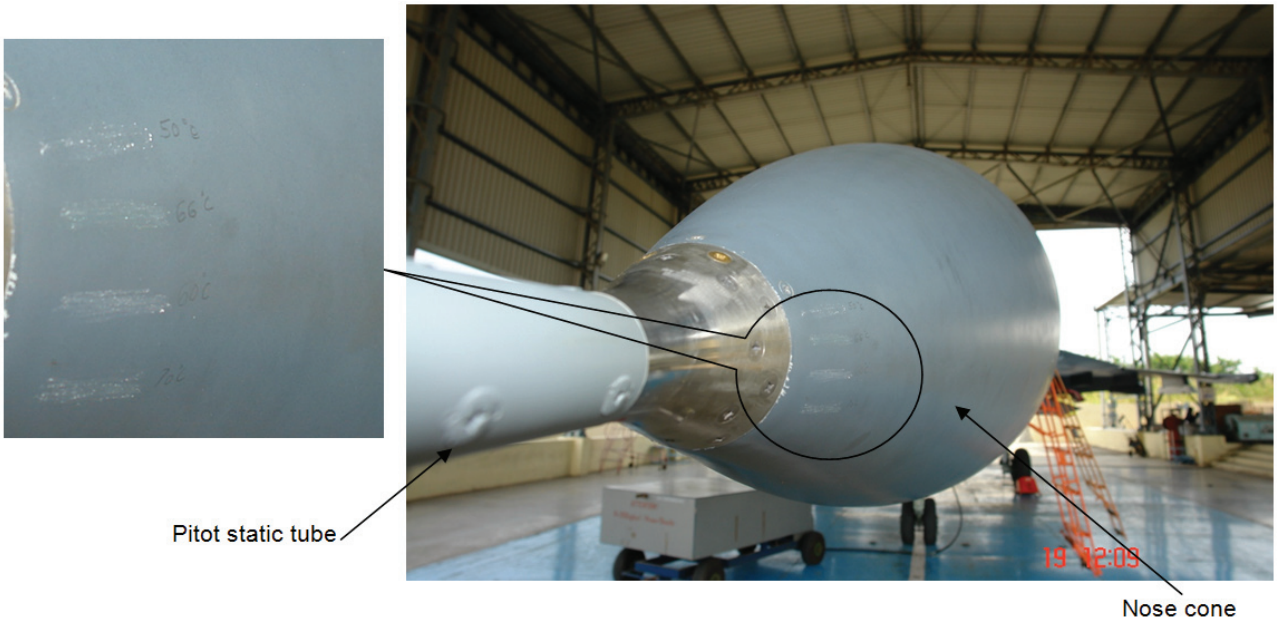

Figure 5. Sample marking line of thermal crayon aft of nose tip at flight profile 1.

2.3.1 Uncertainty Analysis of Skin Temperature Measurement using Thermal Crayons

Uncertainty analyses of skin temperature measurement for thermal crayons of temperature 38 °C, 40 °C, 43 °C, 48 °C, 50 °C, 52 °C, 55 °C, 60 °C, 66 °C, 70 °C, 73 °C, 75 °C, 79 °C, and 80 °C have been undertaken to incorporate the quantification of doubt about measurement results. Outer plane surface of an oven was selected for this analysis as this was not practically possible during flight sortie. Measurement of the temperature by thermal crayons has been validated by simultaneous measurement of temperature using infrared thermometer for uncertainty analysis. Study by Burns[4] was undertaken in this context which describes newly developed screening methodology and tools for early assessment of deep retrofit potential across the entire DoD stock of 250,000 buildings where sensitivity and uncertainty analyses tools are used to isolate critical design parameters and to establish performance bounds during design.

2.3.1.1 Experimental Setup for Online Recording of Temperatures by Thermal Crayon and Infrared Thermometer

To simulate the thermal heating of fuselage skin by ram air, the outer surface of shaft furnace has been identified as a heat source. The uniform temperature from 38 °C to 80 °C is maintained in a stepwise manner at the outer surface of furnace due to convective heat transfer by inner core of furnace which was maintained at the temperature of 200 °C - 250 °C. Thermal crayon of temperature 38 °C, 40 °C, 43 °C, 48 °C, 50 °C, 52 °C, 55 °C, 60 °C, 66 °C, 70 °C, 73 °C, 75 °C, 76 °C, 79 °C, and 80 °C were drawn at the outer surface of furnace. Melting of a particular thermal crayon indicates the temperature achieved at that time. Simultaneously, to verify this temperature (for measurement accuracy) an infrared thermometer was used. Temperature measurements have been taken at a distance of approx. 1 feet from test specimen of thermal crayon. infrared thermometer is capable of measuring point temperature.

Schematic diagram and actual experimental setup is shown in Fig. 6.

2.3.1.2 Recording of Data by Thermal Crayons and Infrared Thermometer

Ten readings of thermal crayons markings of each temperature were taken to have a better estimate of true value as suggested by Bell[5]. Stephanie Bell stated that, a standard uncertainty is a margin whose size can be thought of as 'plus' or 'minus' one standard deviation. The standard uncertainty (*u*) tells about the uncertainty of an average (not just about the spread of values). When a set of several readings *(n)* has been taken, particular value of reading is abbreviated as x_i ,the mean (x_{mean}), then the estimated standard deviation (*s*) can be calculated for the set.

The estimated standard uncertainty $(u) = s/\sqrt{n}$

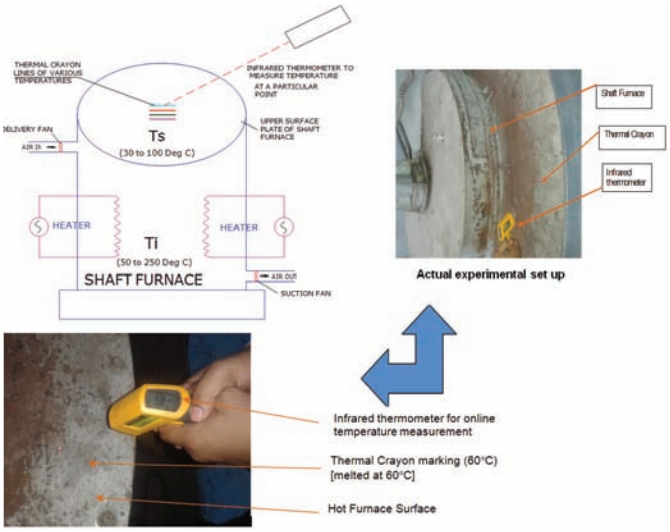

Figure 6. Schematic diagram and actual experimentation for uncertainty analysis.

where s= Standard deviation = $\sqrt{(\sum_{i=1}^{n}[(x_i - x_{mean})^2/(n-1)]}$

The results of uncertainty analysis of recorded temperatures by thermal crayons and laser gun at 38 °C, 40 °C, 43 °C, 48 °C, 50 °C, 52°C, 55°C, 60°C, 66 °C, 70 °C, 73 °C, 75 °C, 79 °C and 80 °C are shown in Table 1.

2.3.2 Flight Tests

To validate the results obtained from CFD analysis, three flight tests were carried out for flight profiles 1, 2, and 3. The flight parameters were analysed using flight data recorder (FDR). FDR data shows the variations in ambient temperature 40.4 °C, 44.3 °C, 38.8 °C, and 42.4°C at altitudes of 1175.2 m, 1041.1 m, 1205 m, and 1070.9 m, respectively (Fig. 7).

The temperature achieved at a particular zone was analysed by melting of thermal crayon at a particular temperature. The temperature achieved at these zones in flight tests 1, 2, and 3 are shown in Table 2.

The average temperature of the cockpit surfaces has been calculated by averaging the temperatures at eight identified locations as mentioned in Table 2. The average cockpit surface temperature at flight profiles 1, 2, and 3 are estimated as 49.75°C, 50.375°C, and 49.5°C, respectively. It is difficult to obtain the first/ second decimal place precision using thermal crayons due to their limitation of measurement accuracy but it gives a fair idea of comparative results of CFD analysis and flight tests. The average cockpit surface temperature obtained from flight tests was compared with CFD and theoretical results of our previous research[1]. The comparison of skin temperature predicted by CFD and theoretically shown in Table 3.

The skin temperatures evaluated by CFD and flight tests are in close agreement with each other.

The percentage deviation of skin temperature estimated by CFD with flight test results is observed as 4.32 per cent, 5.07 per cent and 4.04 per cent at flight profiles 1, 2, and 3, respectively.

Table 1. Summary of results of uncertainty analysis of recorded temperatures by thermal crayons and laser gun

Temperature recorded by thermal crayon (°C)	Arithmetic mean of temperature recorded by laser gun (°C)	Standard deviation (s) $=\sqrt{(\sum_{i=1}^{10}[(x_i - x_{mean})^2/(n-1)]}$ (°C)	Standard uncertainty $(u) = s/\sqrt{n}$ here n=10 (°C)	Expected temperature with uncertainty (°C)	Expected percentage error in measured temperature considering uncertainty
38	38.18	0.2699	0.0853	38.18±0.0853	±0.22 %
40	40.13	0.2983	0.09434	40.13±0.9434	±0.23%
43	43.25	0.3503	0.1108	43.25±0.1108	±0.26%
48	47.96	0.4299	0.1359	47.96±0.13597	±0.28%
50	50.06	0.3339	0.1056	50.06±0.1056	±0.21%
52	52.11	0.3381	0.1069	52.11±0.1069	±0.20%
55	55.14	0.3098	0.0979	55.14±0.0979	±0.18%
60	60.15	0.3027	0.0957	60.15±0.09574	±0.16%
66	66.27	0.3128	0.0989	66.27±0.0989	±0.15%
70	69.98	0.4104	0.1297	69.98±0.1297	±0.19%
73	73.23	0.2907	0.0919	73.23±0.09195	±0.13%
75	75.40	0.2699	0.0853	75.12±0.08537	±0.11%
79	79.15	0.2798	0.0885	79.15±0.08850	±0.11%
80	79.89	0.3844	0.1215	79.8±0.1256	±0.15%

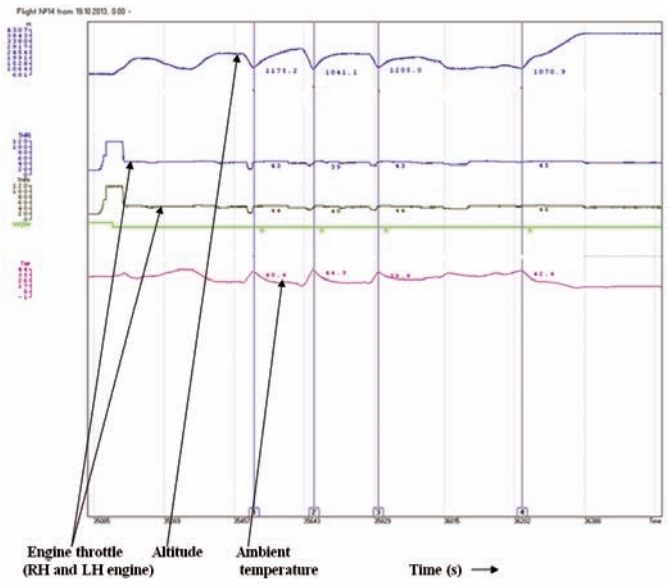

Figure 7. Variation of ambient temperature w.r.t time.

3. GOVERNING EQUATIONS TO CALCULATE OPTIMISED COCKPIT HEAT LOAD

Using skin temperature derived from CFD and theoretical analyses. Following heating sources were considered to estimate cockpit heat load:

Aerodynamic heating through side walls (Q_1), heat Transfer through front bulk head (Q_2), heat transfer through rear bulk heads (Q_3),heat Transfer through cockpit floor (Q_4), convective and radiation heating through structural projections (Q_5), aerodynamic heating through windshield (Q_6), aerodynamic heating through canopy (Q_7), radiation heat transfer through transparencies (canopy and windshield) (Q_8), metabolic heat loads of pilots (Q_9),heat transfer due to avionics and electrical equipment (Q_{10}). Sectional view of cockpit side wall are shown in Fig. 8.

3.1 Aerodynamic Heating through Cockpit Side Walls

Heat transfer through metallic cockpit side wall is by means of conduction and convection. To simplify calculations, an overall heat transfer coefficient was calculated and then the heat that is given to the cockpit was determined using following equation.

$$Q_1 = U_1 * A_{side} * (T_{skin} - T_{cabin}) \quad (1)$$

where

$$U_1 = \left(1/h_{ram} + b_{skin}/k_{skin} + 1/h_g + (b_{gw} * f)/k_{gw} + 1/h_{cabin}\right)^{-1}$$

Cockpit heat loads were calculated at skin temperatures (T_{skin}) 337.807 K, 320.6 K, 320.82 K, and 320.50 K (As per derived results in research mentioned at[1]).

Sample calculation at theoretical skin temperature 337.807K is placed below:

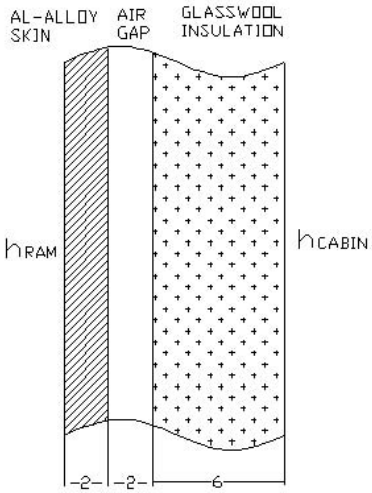

Figure 8. Cross-sectional view of cockpit side wall.

Table 2. Recorded skin temperature during flight tests

Location of marking of thermal crayons	Skin temperature during flight test-1 for flight profile 1 (°C)	Skin temperature during flight test-2 for flight profile 2 (°C)	Skin temperature during flight test-3 for flight profile 3 (°C)
Aft of nose tip	50	50	50
Nose cone	52	55	48
Entrance of wind shield	50	50	50
Wind shield	48	50	50
Canopy	50	50,	50,
Cockpit skin	50	50	50
Aft of cockpit	48	48	48
Fin portion	50	50	50
Average temperature	**49.8**	**50.4**	**49.5**

Table 3. Comparison of skin temperature obtained during theoretical, CFD, and flight tests analyses

Analyses	Average skin temperature during flight test-1 for flight profile 1	Average skin temperature during flight test-2 for flight profile 2	Average skin temperature during flight test-3 for flight profile 3
Theoretical	64.8	64.8	64.8
CFD	47.6	47.8	47.5
Flight tests	49.8	50.4	49.5

Calculations of estimation of h_{ram} ,h_g and h_{cabin} are shown in Table 4.

$U_1 = \left(1/h_{ram} + b_{skin}/k_{skin} + 1/h_g + \left(b_{gw} * f\right)/k_{gw} + 1/h_{cabin}\right)^{-1}$

$=(1/443.50+2x10^{-3}/177+1/17.24+(0.006*0.33/0.0548)+1/18.77)^{-1}$ =6.681 W/m^2 K

Area of sidewalls = 5.49m^2

$Q_1 = U_1 * A_{side} * \left(T_{skin} - T_{cabin}\right)$ = 6.681* 5.49* (337.94 - 301) = 1354.9W.

3.2 Heat Transfer through Front Bulkhead (Q_2)

Heat is generated in the space in front of the front bulkhead due to the instruments stored in the bay. This heat is conducted via the metallic front bulkhead into the cockpit.

$$Q_2 = U_2 * A_{bulk} * \left(T_{bay} - T_{cabin}\right) \quad (2)$$

where $U_2 = \left(1/h_{bay} + b_{bulk}/k_{bulk} + 1/h_{cabin}\right)^{-1}$

We need to calculate the value of equivalent heat transfer coefficient through the bay h_{bay}

Calculation of h_{bay}:

Table 4. Calculation of h_{ram}, h_g and h_{cabin}

Parameter	Calculations with description
Calculation of h_{ram}	In high speed boundary layer as per method, known as the *reference temperature method is* described in detail by Eckert[6] . The final value of h_{ram} is calculated using following relationship: $\left(m_{FP1}\right)_{CFD} = 0.7353\, m_{th}$ **Reference temperature T* =337.807 K** Reference pressure $P^* = (T^* / T_¥)^{g/g-1} * P_h$ = $((337.807/313)^{1.4/1.4-1}) * (0.9623*10^5)$ =1.2567*10^5 N / m^2 Density at P* $\rho^* = \left(P^* / RT^*\right)$ ρ^* = 1.2567*10^5 / 287* 337.807 = 1.296 kg/m^3 Characteristic length (D) is taken as diameter of cockpit as it shortest for the flow over the cockpit surface. Here, diameter of cockpit : 1.93 m $Re^* = \left(\rho^*\right) * V_{true} * D / \mu^*$ = (1.296*283.702*1.93) / (1.67*10^{-5}) = 4.43* 10^7 Prandtl No. $Pr^* = \left(\mu^*\right) * (C_p^*) / \left(k^*\right)$ = (1.67*10^{-5})*(1.002*10^3)/ 0.026 = 0.644 The following relation by Prandtl-Schlichting measures the average friction factor accurately for Reynolds no. less than 10^9. Average friction factor: $C_f` = 0.455 / \left(\log_{10} Re^*\right)^{2.58}$ = 0.455/ ($\log_{10}$ 4.43*10$^7$)$^{2.58}$ = 0.00240 Local friction factor $C_f = \left(0.557\, C_f`\right) / \left(0.557 + 2 * \sqrt{}\, C_f`\right)$ = 0.00204 Stanton No. $St^* = \left(C_f * S\right) / 2$ where S is a factor such that 1.25≥S≥1.18 for 10^5≤ Re* ≤10^9. For Re* = 4.43*10^7; S = 1.18 Hence $St^* = \left(C_f * S\right) / 2$ = (0.00204 * 1.18) / 2 = 0.001204 Convective heat transfer co-efficient. of ram air h_{ram} $h_{ram} = St * \left(\rho^*\right) * \left(C_p^*\right) * V_{true}$ = 0.001204* 1.296 * 1002 * 283.71 Thus, **h_{ram} = 443.58 W/m^{2}K**
Calculation of h_{cabin}	As per SAE Aerospace Applied thermodynamics manual[7], h_{cabin} is calculated by the following empirical formula considering inside mean velocity 3.3 ft/sec. $\left(h_{cabin}\right)_{F.P.S} = 2 + \left(0.314\, V_{mean}\right)$ where h_{cabin} is in terms of Btu/ hr-ft^2-°F and V_{mean} is in ft/s $(h_{cabin})_{S.I.}$ = 5.6782 * $(h_{cabin})_{F.P.S}$ = 5.6782* (2 + (0.314 *3.3))= **17.24015** W/m^{2}K
Calculation of h_g	$h_g = h_{gr} + h_{gc}$ From convective heat transfer coefficient chart : At average air gap temp: (337.807+301)/2 = 319.40K=64.807 °C h_{gr} = 0.4 CHU/hr ft^2 °C and h_{gc} =2.5 CHU/hr ft^2 °C $h_g = h_{gr} + h_{gc}$ = 0.4 +2.5 =3.3 CHU/hr ft^2 °C = **18.77 W/ m^2 °C.**

The value of h_{bay} is assumed to be 1.5 CHU/hr ft^2 °C, which is determined experimentally for aircraft bay area

h_{bay} = 1.5 * 5.6925 W/m^{2}K = 8.53875 W/m^{2}K

$Q_2 = U_2 * A_{bulk} * (T_{bay} - T_{cabin})$ = 5.7119 * 0.629 *(325.473- 301) = 87.92W.

In a similar way heat transfer through rear bulk head (Q_3), heat transfer through cockpit floor (Q_4), convective and radiation heating through structural projections (Q_5), aerodynamic heating through windshield (Q_6), aerodynamic heating through canopy (Q_7), radiation heat transfer through transparencies (canopy and windshield) (Q_8) and heat transfer due to avionics and electrical equipment (Q_{10}) have been calculated. Metabolic heat load of pilots has been taken as 300W for 2 pilots (150W per pilot).

Thus, the total heat load in the cockpit is given by $\sum Q_n$

$Q_{total} = Q_1 + Q_2 + Q_3 + Q_4 + Q_5 + Q_6 + Q_7 + Q_8 + Q_9 + Q_{10}$

= 6815.31 Watts

The distribution of constituents of theoretical cockpit heat load is shown in Fig. 9.

3.3 Comparison of estimated Cockpit Heat Load using Skin Temperatures

Derived by CFD analysis and flight tests. In a similar manner, cockpit heat load has been calculated using skin temperatures derived by CFD and Flight test analysis for flight profile-1, 2 and 3. The variation of average cockpit heat load w.r.t average skin temperature during CFD analysis and flight tests is shown in Table 5.

4. ESTIMATION OF BLEED AIR

To maintain Cockpit mean temperature of 28 °C at theoretical cockpit heat load. Assuming turbocooler outlet air temperature is 5° C. At cockpit heat load of 6815.31 W, the mass flow rate of ECS bleed air required at the inlet turbocooler, which will be delivered to cockpit after cooling, is estimated as

$$Q = m * CpDT \quad (3)$$

6815.13 = m *1005 (28- 5)

m=0.2964 kg/s = **1061.41** kg/h

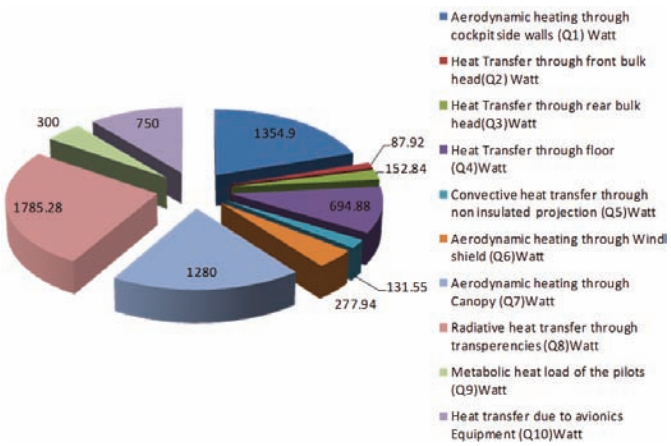

Figure 9. Distribution of constituents of theoretical cockpit heat load.

Table 5. Variation of average cockpit heat load w.r.t average skin temperature during CFD analysis and Flight tests

Analysis	Profile no	Average skin temperature (°C)	Average cockpit heat load (W)
CFD	Flight Profile 1	47.6	5011.62
	Flight Profile 2	47.82	5033.29
	Flight Profile 3	47.5	5001.79
Flight tests	Flight Profile 1	49.75	5223.80
	Flight Profile 2	50.375	5285.48
	Flight Profile 3	49.5	5199.13

4.1 Bleed Air Requirement at Flight Profiles 1, 2, and 3 (Based on Estimation of Cockpit Heat Loads)

Similarly, bleed air requirement for cockpit heat load of flight profiles 1, 2, and 3 for maintaining cockpit mean temperature of 28°C has been calculated for theoretical, CFD, and flight test analyses. Bleed air requirement for heat loads based on CFD results for flight profiles 1, 2, and 3 are estimated as 780.52 kg/h, 783.9 kg/h, and 778.99 kg/h, respectively. This shows there is average 26 per cent reduction in bleed air requirement when CFD results were compared with theoretical results. Bleed air requirement for heat loads based on flight test results for flight profiles 1, 2, and 3 are estimated as 813.57 kg/h , 823.17 kg/h, and 809.72 kg/h, respectively.

5. EFFECT OF REDUCTION IN BLEED AIR ON PERFORMANCE OF AIRCRAFT

Extraction of bleed air from engine plays a significant role in affecting net thrust, specific fuel consumption, fan turbine inlet temperature, bleed total pressure and bleed total temperature. The study has been undertaken to understand these effects by literature review on two research papers:

- The effects of compressor seventh stage bleed air extraction on performance of the F100-PW-220 afterburning Turbofan engine by Evans[8]
- Effect of compressor outlet air bleed on performance of a centrifugal flow turbojet engine with a constant area jet nozzle by Huntley[9].

In the study by Evans[8], Pratt[10] and Whitney steady state mathematical model by Pratt and Whitney Aircraft Group, F100 engine model derivative program,1980[10] was used to determine the response of the F100-PW-220 engine to the various levels of interstage bleed. The research by Evans predicts the following:

- For each additional percentage of bleed, there is -6.66 °C rise in fan turbine inlet temperature.
- The first 1 per cent of bleed results in a reduction of approximately 3 per cent of bleed pressure. The second percent of interstage bleed causes about 8 per cent reduction in bleed pressure. For 2.6 per cent bleed, approximately 15 per cent of compressor interstage bleed pressure is lost.
- Compressor interstage bleed has little effect on compressor inter stage bleed temperature. For the maximum bleed of 2.6 per cent, there is only -12.22 °C changes.

At flight conditions, when engine is operating below fan turbine inlet temperature (FTIT), increasing bleed has only 0.2 per cent loss in thrust per percentage of interstage bleed. For maximum 2.6 per cent of interstage bleed, there is a reduction of 6 per cent of thrust.

In the study by Huntley,[9] the effect of compressor outlet air bleed on turbojet engine performance is calculated using analysis based on experimentally determined component characteristics of a centrifugal flow turbojet engine with a constant area jet nozzle. The effect of air bleed on the pumping characteristics of a centrifugal turbojet engine has been presented for a range of engine speeds from 0.9 to 1.0 of rated engine speed at a flight Mach No of 0.52 and altitude of 7315.2 m flow. This analyses is limited to fixed-configuration engines including fixed-area jet nozzles operating within the region of a choked jet nozzle. An analytical method of performance evaluation with compressor outlet air bleed has been published by Hensley[11,] which presents a general method of component matching and includes generalized working charts for an axial flow turbojet engine. The effect of compressor outlet air bleed on specific modes of engine operation was then determined using charts by Rom[12], *et al.* The performance of a centrifugal flow turbojet engine with compressor outlet air bleed would be expected to be different from that of an axial flow turbojet engine because of the basic difference in compressor characteristics. The engine component characteristics were obtained directly from experimental information available on a centrifugal flow turbojet engine. In addition, compressor characteristics were available from experimental information obtained from a similar compressor on unit test rig. Complete recovery of ram pressure was assumed. The turbine and jet nozzles were considered to be choked for all conditions over the limited range of engine speeds considered. A turbine efficiency of 79 per cent was used and was considered independent of engine speed or compressor outlet air bleed. A simplified representation of the combined turbine and fixed-area jet nozzle has been presented by Sutor[13].

The research by Hensley[11] predicts the following:

- Specific fuel consumption (SFC) increases on an average of 2 per cent for each percentage of increased bleed for constant engine speed.
- The maximum net thrust decreases at a rate of about 2.5 per cent for each per cent of air bleed.

6. RESULTS AND DISCUSSION

The average skin temperatures calculated by CFD analysis and flight trials have been considered as benchmark to calculate the optimised heat load as significant variation of -26.70 per cent (max) in average cockpit skin temperature estimated by theoretical and CFD analyses have been observed. Further, it can be inferred that CFD and flight test results are in close agreement with each other with maximum variation of -5.07 per cent in average skin temperature. Hence, average skin temperature calculated by CFD is definitely helpful and realistic for optimisation of cockpit heat load. CFD analyses predicts average skin temperature of 47.6 °C, 47.82 °C, and 47.5 °C at flight profiles 1, 2, and 3 respectively, however theoretically it has been calculated as 64.807 °C (which is independent of AoA). Cockpit heat load at skin temperature 64.807 °C is calculated as 6815.31 W. The cockpit heat loads at skin temperature of 47.6 °C, 47.82 °C, and 47.5 °C are estimated as 5011.62 W, 5033.29 W, and 5001.79 W respectively. Flight tests analyses predict average skin temperature of 49.75 °C, 50.375 °C and 49.5 °C at flight profiles 1, 2, and 3 respectively. The cockpit heat loads at skin temperature of 49.75 °C, 50.375°C and 49.5°C are estimated as 5223.80 W, 5285.48 W and 5199.13 W, respectively. As average skin temperature estimated by CFD and flight tests are in close agreement with each other, hence cockpit heat load calculated using average skin temperature of CFD results/ flight tests can be considered as optimum cockpit heat load. CFD analysis shows that minimum cockpit heat load of 5001.79 W observed at 313K, 0.8M ,+7 deg AoA (flight profile 3) while maximum cockpit heat load of 5033.29W is observed at 313K, 0.8M, -7° AoA (flight profile 2). Cockpit heat load of 5001.79 W at 313K, 0.8 M, 0 deg AoA (flight profile 1) is in between the cockpit heat load estimated at flight profiles 2 and 3. The cockpit heat load estimated on these three profiles can beconsidered as optimised heat load. Based on optimised cockpit heat load analysis, estimation of bleed air requirement to maintain cockpit mean temperature 28°C has been carried out. At theoretical cockpit heat load of 6815.31 W, there is a requirement of 1061.41 Kg/hr of bleed air to maintain cockpit mean temperature 28 °C. Similarly, at cockpit heat load of 5011.62 W, 5033.29 W, 5001.79 W, 5223.80 W, 5285.48 W, and 5199.13 Watt, there is a requirement of 780.52 kg/h, 783.9 kg/h, 778.99 kg/h, 813.57 kg/h, 823.17 kg/h, and 809.72 kg/h of bleed air, respectively. This shows there is average 26 per cent reduction in bleed air requirement when we compare CFD results with theoretical results. It can be seen that flight tests have predicted slightly more skin temperature as compare to CFD analysis. Hence, cockpit heat loads estimated by CFD analysis (based on estimated skin temperature) are less than by 23 per cent as compared to flight tests

6.1 Analysis on Distribution of Constituents of Cockpit Heat Load

The analysis of cockpit heat load in theoretical, CFD and flight tests shows that radiation heat transfer through transparencies contribute the maximum part of heat load (26 per cent to 35 per cent). Second and third major contributors of heat loads are aerodynamic heating through cockpit side wall (13 per cent to 19 per cent) and canopy (13 per cent to 18 per cent), respectively. By the reduction of projected area of transparencies, radiation heat transfer can be reduced which can reduce overall cockpit heat load drastically.

6.2 Generation of Governing Equation for the Variation of Cockpit Heat Load with Skin Temperature Predicted by CFD Analysis and Flight Tests

The focus of this study is to generate governing equations of variation of cockpit heat load w.r.t variation in skin temperature. CFD analysis has predicted the skin temperatures at flight profiles 1, 2, and 3. Using these skin temperatures, estimation of cockpit heat loads is carried out. The cockpit heat loads at skin temperature of 47.6 °C, 47.82°C, and 47.5 °C are estimated as 5011.62 W, 5033.29 W, and 5001.79 W respectively. The polynomial trend line of 2nd order has been

drawn at cockpit head load variation and following governing equation of variation of cockpit heat load w.r.t skin temperature has been derived

Cockpit heat load $(y) = 0.625\,X^2 + 38.86\,X + 1745$ (4)

Similarly, the following governing equations of variation of cockpit heat load w.r.t skin temperature has been derived by conducting flight test:

Cockpit heat load $(y) = 0.009\,X^2 + 97.77\,X + 336.9$ (5)

where y is Cockpit Heat load in X isCockpit skin temperature.

These governing equations will help the user to directly estimate the cockpit heat load at a particular skin temperature when aircraft flies within critical flight regimes (i.e flight profiles 1 to 3).

The variation of cockpit heat load w.r.t skin temperature predicted by CFD analysis and flight tests are shown in Figs. 10 and 11 respectively.

Actual cockpit heat load variation w.r.t skin temperature will lie in between the cockpit heat load variation evaluated by CFD and flight trials.

6.3 Governing Relationships between Cockpit Heat Loads and Bleed Air Requirements

The following relationships have been derived

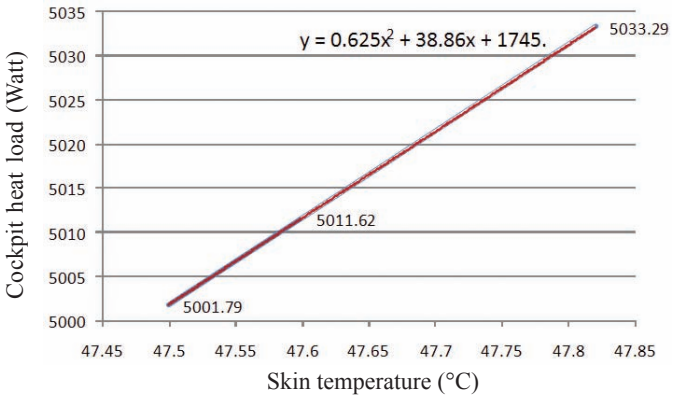

Figure 10. Cockpit heat load variation w.r.t. skin temperature at flight profiles 1, 2, and 3 (estimated by CFD analysis).

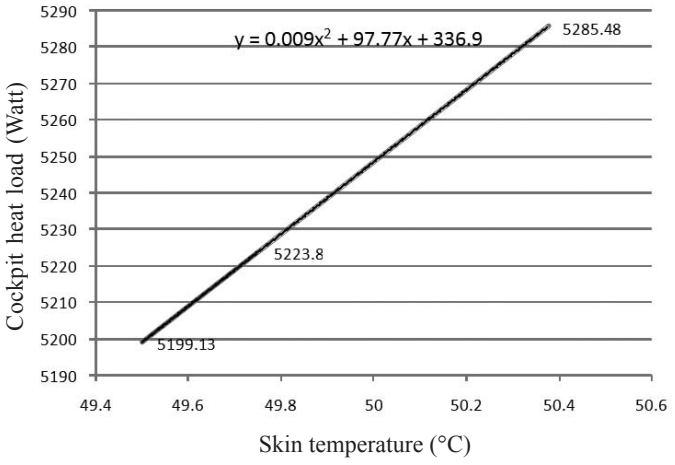

Figure 11. Cockpit heat load variation w.r.t. skin temperature at flight profiles 1, 2, and 3 (estimated by flight tests).

6.3.1 Relationship between theoretical cockpit heat load (Q_{th}) and estimated cockpit heat load (using skin temperature estimated by CFD analysis) for flight profile 1(Q_{FP1}), flight profile 2(Q_{FP2}) and flight profile 3 (Q_{FP3})

Relationship between Q_{FP1} and Q_{th}

$$(Q_{FP1})_{CFD} = 0.7353\,Q_{th}$$

Relationship between $Q_{FP2\ and}Q_{th}$

$$(Q_{FP2})_{CFD} = 0.7385\,Q_{th}$$

Relationship between Q_{FP3} and Q_{th}

$$(Q_{FP3})_{CFD} = 0.7339\,Q_{th}$$

6.3.2 Relationship between cockpit heat loads estimated by CFD analysis and flight tests for flight profile 1, flight profile 2, and flight profile 3:

Relationship between $(Q_{FP1})_{FT1}$ and $(Q_{FP1})_{CFD}$

$$(Q_{FP1})_{FT1} = 1.042\ (Q_{FP1})_{CFD}$$

Relationship between $(Q_{FP2})_{FT2}$ and $(Q_{FP2})_{CFD}$

$$(Q_{FP2})_{FT2} = 1.050(Q_{FP2})_{CFD}$$

Relationship between $(Q_{FP2})_{FT3}$ and $(Q_{FP3})_{CFD}$:

$$(Q_{FP3})_{FT3} = 1.039(Q_{FP3})_{CFD}$$

The above relationships will help the user to calculate actual cockpit heat load , if theoretical heat load is known or cockpit heat load is derived from Eqns (4) or (5) using skin temperature.

6.3.3 Relationship between maximum possible bleed air requirement (m_{th}) and estimated bleed air requirements estimated by CFD analysis for flight profile 1(m_{FP1}), flight profile 2(m_{FP2}) and flight profile 3 (m_{FP3})

Relationship between m_{FP1} and m_{th} :

$$(m_{FP1})_{CFD} = 0.7353\,m_{th}$$

Relationship between m_{FP2} and m_{th}:

$$(m_{FP3})_{FT3} = 1.039(m_{FP3})_{CFD}$$

$$(m_{FP2})_{CFD} = 0.7385\,m_{th}$$

Relationship between m_{FP3} and m_{th} :

$$(m_{FP3})_{CFD} = 0.7339\,m_{th}$$

6.3.4 Relationship between calculated bleed air requirements (estimated by CFD analysis and flight tests for flight profile 1, 2 and 3)

Relationship between $(m_{FP1})_{FT1}$ and $(m_{FP1})_{CFD}$

$$(m_{FP1})_{FT1} = 1.042\ (m_{FP1})_{CFD}$$

Relationship between $(m_{FP2})_{FT2}$ and $(m_{FP2})_{CFD}$

$$(m_{FP2})_{FT2} = 1.050\ (m_{FP2})_{CFD}$$

Relationship between $(m_{FP1})_{FT3}$ and $(m_{FP3})_{CFD}$

$$(m_{FP3})_{FT3} = 1.039(m_{FP3})_{CFD}$$

The above relationships mentioned at sections 6.3.3 and 6.3.4 will help the user to calculate actual bleed air requirement, if theoretical bleed air requirement is known (derived from theoretical heat load calculations)

6.4 Predicted Increase in Performance Parameters of Aircraft due to Reduction in Bleed Air Requirement based on CFD Results

Assuming there is average 26 per cent reduction in bleed air requirement when we compare CFD results with theoretical results. Based on study conducted by Evan[9], the following improvements in performance parameters are predicted:

- Increase in bleed air pressure: 78 per cent { Assuming minimum 1 per cent increase of bleed pressure per cent of bleed air extraction},
- Increase in thrust : 60 per cent { Assuming increase of 6 per cent thrust per 2.6 per cent reduction in bleed air},
- Decrease in specific fuel consumption (SFC) : 40 per cent { Assuming decrease of SFC 4 per cent per 2.6 per cent reduction in bleed air}. However, there is need to validate these predictions by undertaking experimentations in future.

7. CONCLUSIONS

This research project has evolved a new methodology and simplified approach to estimate optimised cockpit heat load by calculating skin temperature at variable angle of attack, variable altitudes and flight speeds using CFD and flight tests with fair accuracy. Estimation of optimised heat load is impossible in these flight conditions using conventional method (i.e, reference temperature method suggested by Eckert) as effect of angle of attack and boundary layer cannot be included in conventional method during estimation of skin temperature. To get the better results for estimation of skin temperature, it is important that geometry of the mesh is to be appropriately selected based on the application. With extensive literature survey and fair good iterations the geometry of mesh and scale factor, it was decided. The results of fluent analysis shows that the skin temperature remains 0.9472 times of the actual stagnation temperature.

Skin temperature estimated by CFD analysis in flight profiles 1, 2, and 3 has been validated by conducting flight tests. The skin temperatures estimated by flight test are higher by + 5.07 per cent w.r.t skin temperature estimated by CFD analysis. Uncertainty analysis of skin temperature measurement for thermal crayons of various temperatures has been undertaken to incorporate the quantification of doubt about measurement results by thermal crayons. Expected percentage error in measured temperature range (48°C to 52°C) considering uncertainty is estimated as ±0.28 per cent (max). The estimated skin temperature using CFD analysis in three critical flight profiles has been used as input parameter for calculation of optimised cockpit heat load. The theoretical estimated cockpit heat load is compared with cockpit heat load estimated using CFD analysis and flight test in flight profiles 1, 2, and 3. By analysis, it is estimated that the average actual cockpit heat load (estimated by CFD analysis) is 0.7359 (5015.56/6815.31) times that of maximum theoretical heat load. While, average actual cockpit heat load (estimated by flight tests) is 0.7682 times (5236.13/6815.31) that of maximum theoretical heat load.

This research has generated governing equation of variation of cockpit heat load w.r.t skin temperature for critical flight profiles. Relationships between maximum possible bleed air requirement by theoretical analysis, estimated bleed air requirements by CFD analysis and flight tests analysis for critical flight profiles have also been established. This will help the user to calculate actual bleed air requirement, if theoretical bleed air requirement is known. Based on optimised heat load, it is predicted that there is average 26 per cent reduction in bleed air requirement when we compare CFD results with theoretical results, it is predicted that there is Increase in bleed air pressure by 78 per cent, Increase in thrust by 60 per cent and decrease in SFC by 40 per cent This will increase the overall performance of the aircraft. However, there is need to validate these predictions by undertaking experimentations in future.

REFERENCES

1. Gupta, Paresh & Rajput, S.P.S. A computational fluid dynamics (CFD) and thermal analysis to estimate the skin temperature of cockpit surface in various Flight profile. *ASCE J. Aerospace Eng*., 2013, **28**(1), 04014056. doi: 10.1061/(asce)as.1943-5525.0000345
2. Eckert, Ernest R.G. Survey of heat transfer at high speeds. Wright Air Development Centre (WADC), technical Report, 1954, 54-70.
3. Salim & Cheong. Wall y+ approach for dealing with turbulent flow over a surface mounted cube: Part 1 – Low Reynolds number. Seventh International Conference on CFD in the Minerals and Process Industries CSIRO, Melbourne, Australia, 2009.
4. Burns, J.A. A systems approach to high performance buildings: A computational systems engineering r&d program to increase DoD energy efficiency. (SERDP Project EW-1709), 2012.
5. Stephanie, Bell. A Beginner's guide to uncertainty of measurement. National Physical Laboratory, Tedington, Misslessex, UK. ISSN,1999, 2, 1368-6550.
6. Eckert, Ernest R.G. Survey of boundary layer heat transfer at high velocities and high temperatures. Wright Air Development Centre (WADC) Technical report, 1960, 59-624.
7. Aero-thermodynamics systems engineering and design. SAE Aerospace Applied Thermodynamics Manual, Aerospace Information Report (AIR) 1168/3,1989.
8. Evans, Alison B. The effects of compressor seventh stage bleed air extraction on performance of the F-100-PW-220 afterburning turbofan engine. NASA Contractor Report (CR)179447, 1991.
9. Huntley, Sidney C. Effect of compressor outlet air bleed on performance of a centrifugal flow turbojet engine with a constant area jet nozzle. National Advisory Committee for Aeronautics. Technical Note (TN) 2713,1952.
10. Pratt & Whitney. Aircraft Group F100 Engine Model Derivative Program, Preliminary JTF 22B-36 status, prepared for the US Air Force under contract 33657-79-C-0541. West Palm Beach , Users Manual for Deck CCD

1148-0.0, 1980.
11. Hensley, Reece V.; Rom, Frank E. & Koutz, Stanley L. Effect of heat and power extraction on turbojet engine performance. Part I-Analytical method of performance evaluation with compressor outlet air bleed. NACA-TN 2053, 1950.
12. Rom, Frank E. & Koutz, Stanley L. Effect of heat and power Extraction on turbojet Engine performance. Part II-Effect of compressor Outlet Air Bleed for specific modes of engine operation. NACA-TN 2166, 1950.
13. Sutor, Alois T. & Zipkin, Morris A. Method of matching components and predicting performance of turbine propeller engine. NACA-TN 2450,1951.

CONTRIBUTORS

Mr Paresh Gupta has completed his MSc in Aerospace Vehicle Design from Cranfield University, UK, in 2008. Presently, pursuing PhD from Maulana Azad National Institute of Technology, Bhopal. He is presently working as Senior Manager (Design) at Aircraft Upgrade Research and Design Centre, Hindustan Aeronautics Limited, Nasik. He has approximately 14 years of experience in Design and development of Environmental Control System (ECS) of fighter aircraft and presently working as Group Leader of ECS and Fire Fighting Group. He is a recipient of many awards including SODET Award (2011-12) in Gold category for ECS upgrade of MiG 27 aircraft, SODET Award (2013-14) in Bronze category for ECS upgrade of Project Eye Shadow, DARE, DRDO Award for significant contribution of ECS upgrade.

Dr S.P.S. Rajput has completed ME (Thermal engineering) in 1992 and PhD in Refrigeration and Air Conditioning in 2004. He is presently working as Professor at Maulana Azad National Institute of Technology, Bhopal. He has approximately 23 years of teaching and research experience in field of Refrigeration and Air Conditioning system. He has guided 44 M.Tech students. Under his guidance eight PhDs have been awarded and six are under progress. He has published 35 research papers at various international journals and 24 papers at international conferences.